1998

Characterization of Sol-Gel-Derived Cobalt Oxide Xerogels as Electrochemical Capacitors

Chuan Lin
University of South Carolina - Columbia

James A. Ritter
University of South Carolina - Columbia

Branko N. Popov
University of South Carolina - Columbia, popov@engr.sc.edu

Publication Info

Journal of the Electrochemical Society, 1998, pages 4097-4103.

Publisher's link: http://dx.doi.org/10.1149/1.1838920
DOI: 10.1149/1.1838920

11. D. T. Chin and S. Venkatesh, *J. Electrochem. Soc.*, **128**, 1439 (1981).
12. R. Ramanauskas, R. Juskenas, and M. Gladkovas, *Plat. Surf. Finish*, 54 (July 1996).
13. C. Biddulph and M. Marzano, in *Metal Finishing*, 65th Guidebook and Directory Issue, Vol. 95, No. 1A, p. 323 (1997).
14. H. Gedulp, *Zinc Plating*, Finishing Publications Ltd., Middlesex (1988).
15. F. A. Lowenheim, Editor, *Modern Electroplating*, 3rd ed., John Wiley & Sons, New York (1974).
16. M. Smith and A. E. Martell, *Critical Stability Constants*, Vol 4, Plenum Press, New York (1979).
17. A. Rojas and I. Gonzalez, *Anal. Chim. Acta*, **187**, 279 (1986).
18. A. Rojas-Hernandez, M. T. Ramirez, I. Gonzalez, and J. G. Ibanez, *Anal. Chim. Acta.*, **259**, 95 (1992).
19. A. Rojas-Hernandez, M. T. Ramirez, J. G. Ibanez, and I. Gonzalez, *J. Electrochem. Soc.*, **138**, 365 (1991).
20. A. Rojas-Hernandez, M. T. Ramirez, and I. Gonzalez, *Anal. Chim. Acta*, **278**, 321 (1993).
21. A. Rojas-Hernandez, M. T. Ramirez, and I. Gonzalez, *Anal. Chim. Acta*, **278**, 335 (1993).
22. G. J. Hills, D. J. Schiffrin, and J. Thompson, *Electrochim. Acta*, **19**, 657 (1974).
23. S. Fletcher, *Electrochim. Acta*, **28**, 917 (1983).
24. S. Fletcher and G. S. Halliday, *J. Electroanal. Chem.*, **159**, 167 (1983).
25. G. Gunawardena, G. Hills, I. Montenegro, and B. Scharifker, *J. Electroanal. Chem.*, **138**, 225 (1982).
26. W. C. Hsie and J. R. Selman, *Electrochim. Acta*, **30**, 1381 (1985).
27. B. Scharifker and G. Hills, *Electrochim. Acta*, **28**, 879 (1983).
28. A. Serruya, B. R. Scharifker, I. Gonzalez, M. T. Oropeza, and M. Palomar-Pardave, *J. Appl. Electrochem.*, **26**, 451 (1996).
29. G. Trejo, A. F. Gil, and I. Gonzalez, *J. Electrochem. Soc.*, **142**, 3404 (1995).
30. G. Trejo, A. F. Gil, and I. Gonzalez, *J. Appl. Electrochem.*, **26**, 1287 (1996).
31. *1993 Annual Book of ASTM Standards*, Vol. 03.02, *Wear and Erosion; Metal Corrosion*, P. C. Fazio et al., Editors, ASTM G 5. Standard Reference Test for Making Potentiostatic and Potentiodynamic Anodic Polarization Measurements, p. 71, ASTM, Philadelphia, PA (1993).

Characterization of Sol-Gel-Derived Cobalt Oxide Xerogels as Electrochemical Capacitors

Chuan Lin, James A. Ritter,* and Branko N. Popov*

Department of Chemical Engineering, University of South Carolina, Columbia, South Carolina 29208, USA

ABSTRACT

Very fine cobalt oxide xerogel powders were prepared using a unique solution chemistry associated with the sol-gel process. The effect of thermal treatment on the surface area, pore volume, crystallinity, particle structure, and corresponding electrochemical properties of the resulting xerogels was investigated and found to have significant effects on all of these properties. The xerogel remained amorphous as $Co(OH)_2$ up to 160°C, and exhibited maxima in both the surface area and pore volume at this temperature. With an increase in the temperature above 200°C, both the surface area and pore volume decreased sharply, because the amorphous $Co(OH)_2$ decomposed to form CoO that was subsequently oxidized to form crystalline Co_3O_4. In addition, the changes in the surface area, pore volume, crystallinity, and particle structure all had significant but coupled effects on the electrochemical properties of the xerogels. A maximum capacitance of 291 F/g was obtained for an electrode prepared with the CoO_x xerogel calcined at 150°C, which was consistent with the maxima exhibited in both the surface area and pore volume; this capacitance was attributed solely to a surface redox mechanism. The cycle life of this electrode was also very stable for many thousands of cycles.

Introduction

Interest in electrochemical capacitors for high-power devices in energy-storage systems has risen in recent years.[1-5] Moreover, the energy density of the relatively new pseudocapacitor devices that are based on faradaic processes has been reported to be many times greater than that of the more traditional double-layer capacitors.[1-6] Noble metal oxides, such as RuO_2 and IrO_2, have been identified as possibly the best electrode materials for pseudocapacitors. For example, Zheng et al.[7] achieved a remarkable specific capacitance of 760 F/g from a sol-gel-derived amorphous RuO_x with a very high electrical conductivity; but the high cost of this and other noble metal materials may be a limiting factor. Thus, other efforts have aimed at making a lower cost electrode material that has a relatively high capacitance. For example, Liu et al.[8] developed an ultracapacitor device based on a sol-gel-derived porous metal oxide NiO_x/Ni film. The specific capacitance of this device, ranging from 50 to 64 F/g (equivalent to 200 to 256 F/g for a single electrode), is considerably higher than that obtained from carbon-based capacitors. Srinivasan and Weidner[9] also developed an electrochemical route for making nickel oxide capacitors with relatively large specific capacitances of about 240 F/g (from a single electrode). Cobalt oxide electrode materials have also been studied extensively due to a variety of applications in electrocatalysis[10-13] and lithium-ion batteries.[14] However, cobalt oxides have not been examined for use as electrochemical capacitors (with one recent exeption[9]), most likely because the common preparation method, involving the thermal decomposition of a metal salt,[15,16] usually yields low surface area oxides. Even the electrochemical precipitation technique,[9] which produced an acceptable nickel oxide capacitor, resulted in a rather low specific capacitance for cobalt oxide of about 40 F/g (single electrode, fired at 250°C). Nevertheless, it is clear that sol-gel[7,8,17,18] and other precipitation processes[9] have been receiving increasing attention in the electrochemical research community for making high surface area metal oxides.

The sol-gel process is quickly becoming one of the most promising materials synthesis techniques, because it readily allows for control of the texture, composition, homogeneity, and structural properties of the resulting materials.[19] Moreover, numerous studies have been devoted recently to understanding how the synthesis conditions affect the porous structure of sol-gel derived materials.[20-24] But only limited information is available on sol-gel-derived cobalt oxides.[17,25] Also, a paucity of information is available that correlates the surface area and pore structure with the electrochemical properties of the electrode materials.

Therefore, the objective of this work was to develop a new sol-gel synthesis route[26] for making high surface area cobalt

* Electrochemical Society Active Member.

oxide xerogel powders with a controlled pore structure for use as an electrode material in electrochemical capacitors. Another objective was to study the effect of the calcination temperature on the surface area, pore volume, particle structure, and corresponding electrochemical properties of the CoO_x xerogels. Physical adsorption, transmission electron microscopy (TEM), X-ray diffraction (XRD), thermogravimetric analysis (TGA), differential scanning calorimetry (DSC), and electrochemical techniques were used to correlate the electrochemical performance of the material with its physical properties.

Experimental

Reagent-grade cobalt chloride ($CoCl_2$, 98%, Aldrich), sodium ethoxide ($NaOC_2H_5$, 96%, Aldrich), dehydrated ethanol (EtOH, 200 proof, Quantum), ammonium hydroxide (NH_4OH, 50 vol %, Alfa), and potassium hydroxide (KOH, 85% assay, Alfa) were used as received. $CoCl_2$, $NaOC_2H_5$ (mole ratio of $CoCl_2$ to $NaOC_2H_5$ = 1:2) and dehydrated EtOH were added to a three-necked flask equipped with a N_2 purge, cooling water condenser, and magnetic stirrer. The mixture was heated and refluxed for 3 h, and then cooled to room temperature. Next, while agitating, a 0.2 M solution of NH_4OH was added dropwise to form the hydrogel; agitation was continued overnight. The reactions for the synthesis are summarized below

$$CoCl_2 + 2NaOC_2H_5 \rightarrow Co(OC_2H_5)_2 + 2NaCl \quad [1]$$

$$Co(OC_2H_5)_2 + 2H_2O \xrightarrow{NH_4OH} Co(OH)_2 + 2C_2H_5OH \quad [2]$$

In order to remove NaCl from the hydrogel, the gel was washed with a 50 vol % solution of distilled water and EtOH, and vacuum filtered three times. This step was followed by a final wash with dehydrated EtOH. Temperature-programmed drying and calcination in air were used in the final preparation step. With a heating rate of 0.5°C/min, the gel was heated to 65°C and held there for 5 h. It was then heated to 110°C and held there for another 5 h. Finally, it was heated at a rate of 5°C/min to the calcination temperature (varied as a parameter in this study), and held there for 3 h.

The surface area and pore volume were obtained with a Micromeritics Pulse Chemisorb 2700 analyzer, and skeletal densities were measured with a Quatachrome ultrapycnometer 1000. TEM were obtained with a Hitachi H-8000 TEM, and XRD patterns were collected using a Rigaku-D-max B diffractometer equipped with a Cu source. A Perkin-Elmer thermogravimetric analyzer (TGA-7) and a Perkin-Elmer differential scanning calorimeter (DSC-7) were used to determine the weight loss and corresponding thermal effects of the dried gel during calcination in air at a heating rate of 5°C/min.

Cyclic voltammetric and chronopotentiometric measurements were performed with an EG&G PAR model 273 computer-controlled potentiostat-galvanostat, driven by model 273 electrochemical analysis software. A three-electrode system was used for the electrochemical measurements. The working electrode contained about 5 mg CoO_x xerogel bound with 5 wt % polytetrafluoroethylene (PTFE, Aldrich). It was rolled to a thickness of about 100 μm, cut into a circular piece with a diameter of 0.75 cm, and pressed at 3 tons/cm^2 between two pieces of nickel gauze with nickel wire leads for connection. Platinum gauze served as a counter electrode; and a saturated calomel electrode (SCE) was used as a reference electrode. A 1 M KOH solution was used as the electrolyte. All of the electrochemical measurements were conducted at room temperature.

X-ray diffraction peak widths were used to estimate the average size of the crystallite in the CoO_x xerogels from the Scherrer equation[27]

$$d = \frac{K\lambda}{b \cdot \cos\theta} \quad [3]$$

where b is the peak width at its half-height in terms of 2θ, λ is the incident radiation wavelength (1.5406 Å for Cu Kα radiation), θ is the angle of the diffraction, K is a constant (taken as 0.9), and d is the crystallite size. The pore volume and skeletal density measurements were used to obtain the particle density from the following relationship

$$d_p = \frac{1}{V_p + \frac{1}{d_s}} \quad [4]$$

where V_p is the specific pore volume, d_s is the skeletal density, and d_p is the particle density.

Results

The effect of thermal treatment on the surface area and pore volume of the CoO_x xerogels is shown in Fig. 1. The surface area initially increased with an increase in temperature from 110 to 150°C, and it reached a maximum of 198 m^2/g at 150°C. Beyond 150°C, the surface area decreased sharply to about 120 m^2/g at 250°C and 50 m^2/g at 400°C, and finally it reached 20 m^2/g at 600°C. The pore volume exhibited similar trends and increased slightly from 0.40 to 0.43 cm^3/g with an increase in temperature from 110 to 150°C. Beyond 150°C, it decreased linearly with increasing temperature down to 0.04 cm^3/g at 600°C.

The effect of the calcination temperature on the crystalline structure of the CoO_x xerogels is shown in Fig. 2 in terms of the XRD patterns. Between 110 and 150°C the XRD patterns were essentially identical exhibiting only two small featureless peaks at 2θ = 32 and 58°, which were probably associated with amorphous $Co(OH)_2$. At higher temperatures, the XRD patterns exhibited the characteristic peaks of Co_3O_4 [17] at 36.6, 59.2, and 65.1°, which first appeared following calcination at 200°C; and as the temperature increased the intensities of the peaks increased, indicating that more crystallization was taking place. This increase in intensity with an increase in the calcination temperature is also shown in Fig. 3, where the average crystallite size and intensity of the XRD peak at 2θ = 36.6° are plotted as a function of the calcination temperature. Linear relationships were exhibited in both cases. The crystallite size was initially about 4 nm for the CoO_x xerogel calcined at 200°C, and it grew to about 25 nm as the calcination temperature increased to 600°C. The TEM images of the CoO_x xerogels shown in Fig. 4A and B, respectively, were qualitatively consistent with these results. They show that the CoO_x xerogel calcined at 150°C was comprised of 10 nm particles, whereas that calcined at 600°C was comprised of larger 30 to 40 nm particles.

Figure 5 displays the skeletal densities of the CoO_x xerogels calcined at different temperatures. The skeletal density increased slightly from 3.19 to 3.34 g/cm^3 with an increase in temperature from 110 to 150°C, and then it increased linearly to about 5.45 g/cm^3 at 300°C. Between 300 and 600°C, the skeletal density remained essentially constant, and finally it reached 5.74 g/cm^3 at 600°C, which is about 94% of the theoretical density of Co_3O_4.[28] In contrast, the particle

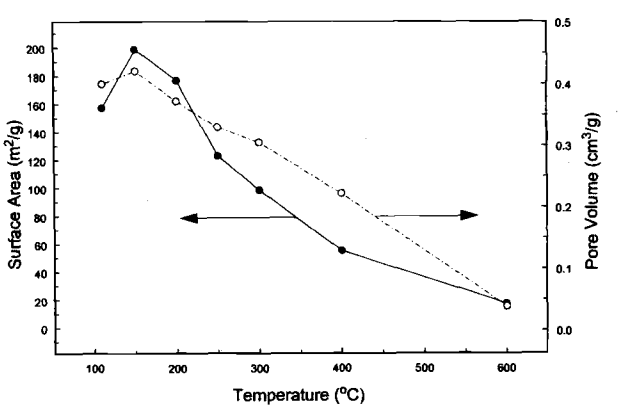

Fig. 1. Effect of the calcination temperature on the surface area and pore volume of the CoO_x xerogels.

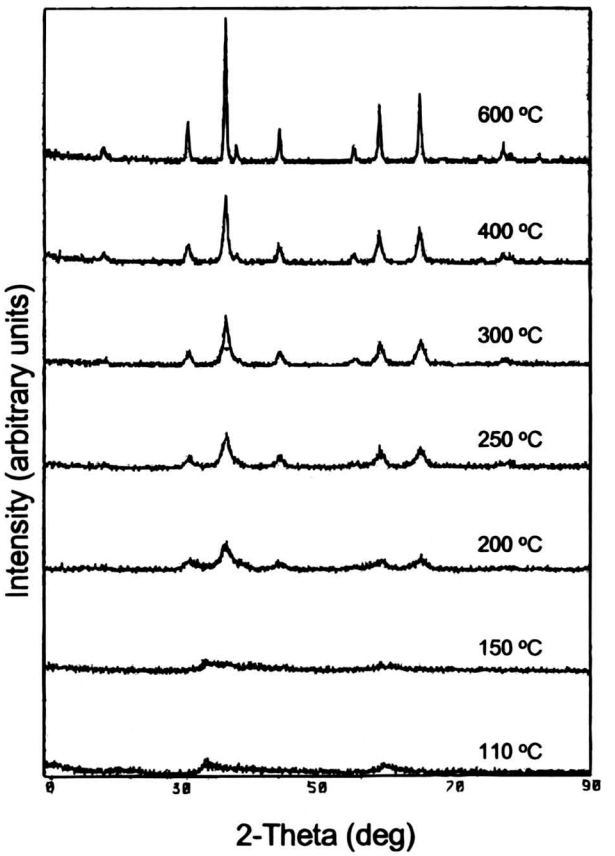

Fig. 2. Effect of the calcination temperature on the XRD patterns of the fresh CoO_x xerogels.

density essentially increased from 3.1 to 4.7 g/cm^3 with an increase in temperature from 150 to 600°C.

The TGA and corresponding DSC analyses are illustrated in Fig. 6. The weight loss of the CoO_x xerogel occurred in three stages: an initial loss of about 13% up to 160°C, followed by a rapid loss of around 14% between 160 and 170°C, and an additional but gradual loss of around 4% up to 750°C. The initial weight loss up to 160°C was not associated with any thermal events as seen in the DSC trace. However, between 160 and 170°C, the weight loss was accompanied by a marked endothermic event that extended over a broader temperature range (up to 270°C) than the weight loss. The final small weight loss between 400 and 650°C was accompanied by another marked thermal event; however, in this temperature range an exothermic event occurred.

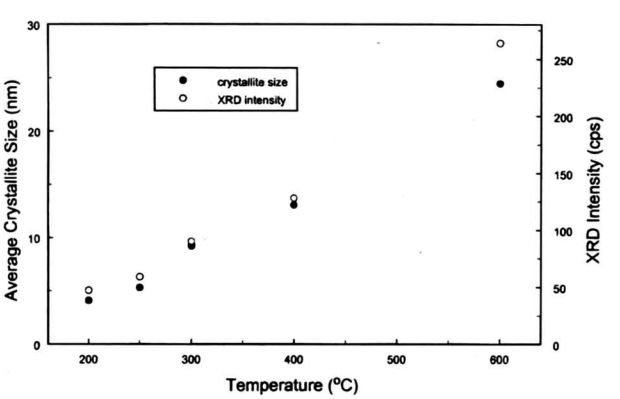

Fig. 3. Effect of the calcination temperature on the average crystallite size and intensity of the fresh CoO_x xerogels from XRD peaks at $2\theta = 36.6°$.

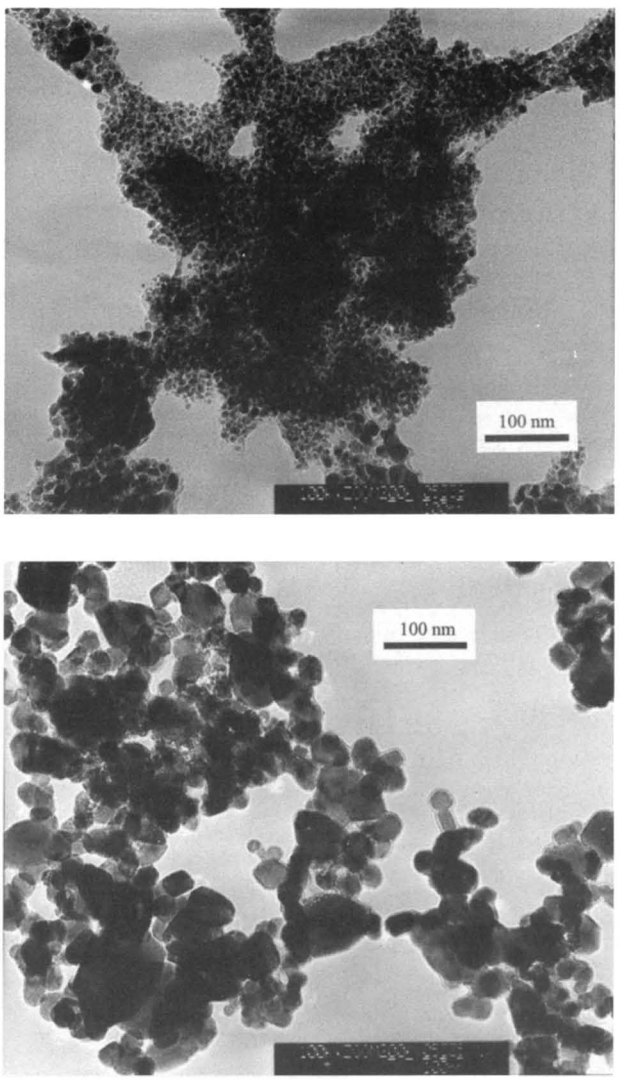

Fig. 4. TEM images of the CoO_x xerogels calcined at (A, top) 150°C and (B, bottom) 600°C.

Cyclic voltammetry (CV) and galvanostatic techniques were used to determine the electrochemical properties of the CoO_x xerogels as a function of the calcination temperature. Figure 7A shows the characteristic shapes of the CV curves for the CoO_x xerogels calcined at three different temperatures (150, 200, and 600°C). The potential was scanned between −0.3 and 0.5 V (vs. SCE) in both directions and the current response was measured for a scan rate of 5 mV/s. In all cases, a single anodic peak was

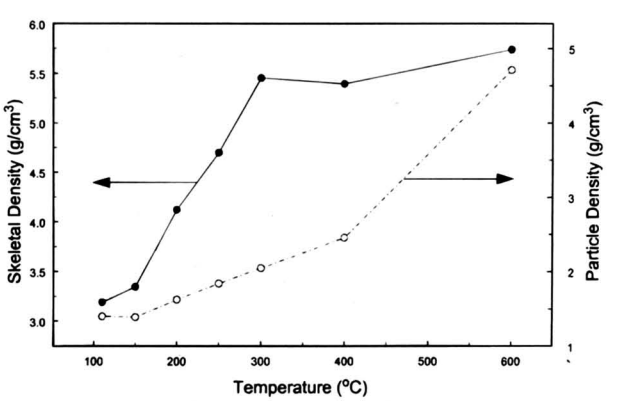

Fig. 5. Effect of the calcination temperature on the skeletal and particle densities of the CoO_x xerogels.

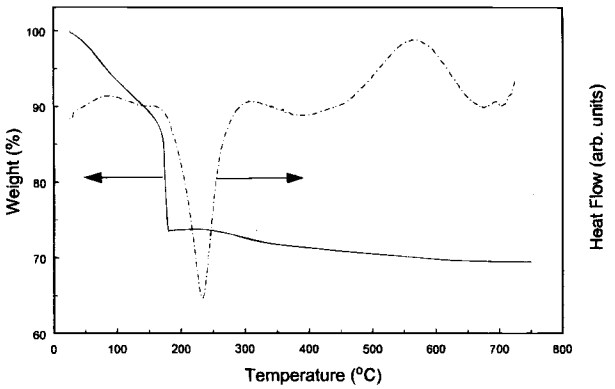

Fig. 6. Thermogravimetric analysis (TGA) and differential scanning calorimetry (DSC) of the CoO_x xerogels heated in air at 5°C/min.

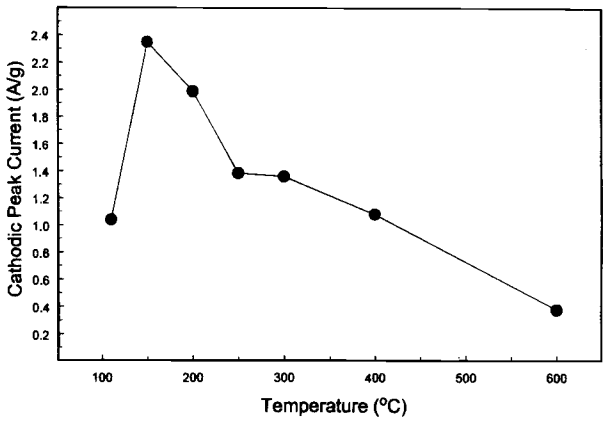

Fig. 8. Effect of the calcination temperature on the cathodic peak currents obtained from the CV results of the CoO_x xerogel electrodes.

exhibited at about 0.45 V, and a corresponding cathodic peak at about 0.30 V. In addition, a shoulder appeared between 0 and 0.3 V for the xerogel calcined at 150°C. The electrochemical stability of the CoO_x xerogel electrode calcined at 150°C was also studied; the result is shown in Fig. 7B. Essentially no change is exhibited in the initial cycle and after several thousand cycles, indicating that this electrode was very stable.

Figure 8 shows the dependence of the cathodic peak current on the calcination temperature. It exhibited a similar trend to the surface area and pore volume plots shown in Fig. 1. A maximum current was obtained for the xerogel calcined at 150°C, which was the same temperature at which the surface area and pore volume exhibited maxima. Constant-current (2.26 mA/cm^2) discharge profiles of the CoO_x xerogels are shown in Fig. 9. The corresponding specific capacitances were calculated from

$$C = \frac{I \cdot \Delta t}{m \cdot \Delta V} \quad [5]$$

and are displayed in Fig. 10. I is the discharge current, Δt is the total discharge time, m is the mass of the CoO_x xerogel, ΔV is the potential drop during discharging, and C is the specific capacitance. The total discharge time was used because it was difficult to determine the transition time for the material calcined at 150°C. In this way, the CoO_x xerogel calcined at 150°C exhibited the highest specific capacitance of 291 F/g. The curves in Fig. 10 also exhibited similar trends to those shown in Fig. 1 and 8; thus, these results were consistent with those obtained from the CVs (Fig. 7A).

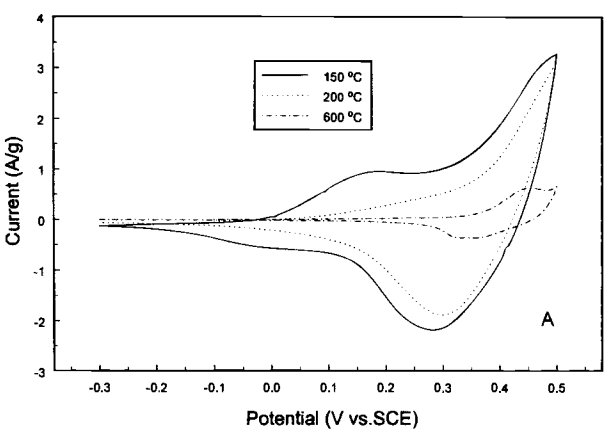

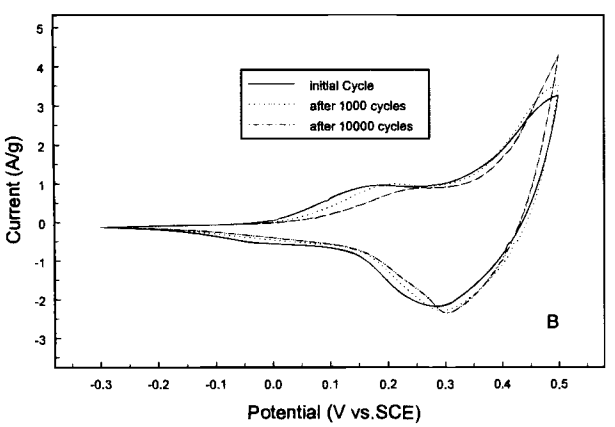

Fig. 7. Cyclic voltammograms (CVs) of (A) the CoO_x xerogels calcined at three different temperatures, and (B) the CoO_x xerogel calcined at 150°C for the first and after several thousand cycles. The curves were normalized to the current response for 1 g of active material; and the CV was measured in 1 M KOH with a sweep rate of 5 mV/s.

Discussion

The chemistry depicted in Eq. 1 and 2 gives rise to unique cobalt oxides via the hydrolysis and condensation of the transition metal alkoxide. However, because the hydrolysis of transition metal alkoxides is so rapid,[19] this chemistry results in sol-gel-derived precipitates instead of gels. Nevertheless, cobalt oxide precipitates can be synthesized with rather interesting physical and electrochemical properties, as discussed above and shown in Fig. 1 to 10.

The increases in the surface area and pore volume from 110 to 150°C (Fig. 1) was attributed to the removal of physisorbed water or some solvent, which may have open-

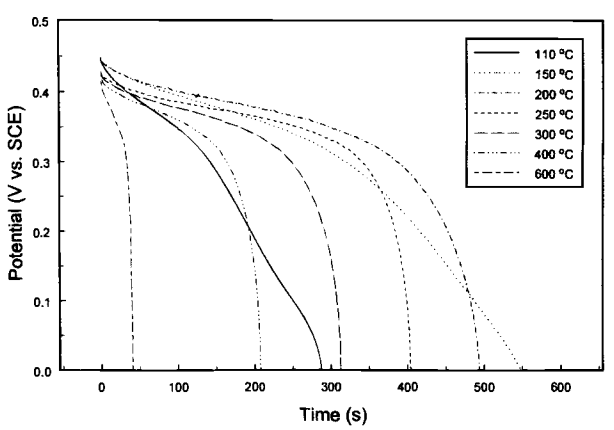

Fig. 9. Effect of the calcination temperature on the constant current discharge curves of the CoO_x xerogel electrodes measured with a current density of 2.26 mA/cm^2 in 1 M KOH solution. The electrodes were approximately 100 μm in thickness and 7.5 mm in diameter, and they contained approximately 4.2 mg of CoO_x xerogel.

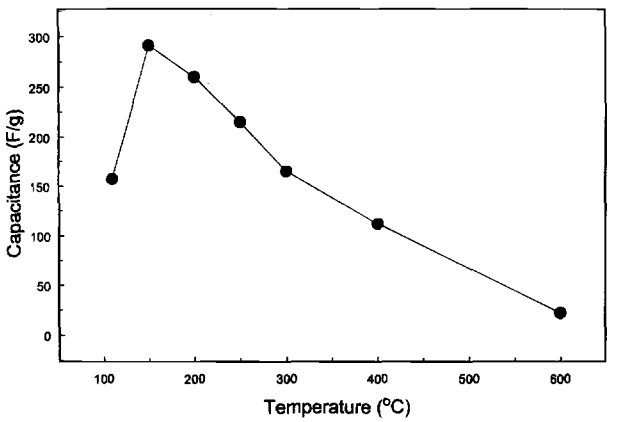

Fig. 10. Effect of the calcination temperature on the specific capacitance of the CoO_x xerogel electrodes.

ed the pore structure of the material.[20] The maxima in both the surface area and pore volume exhibited at 150°C, and the sharp weight loss from 160 to 170°C were most likely due to the decomposition of cobalt hydroxide to form amorphous cobalt oxide by removal of chemisorbed water according to Eq. 6[29,30]

$$Co(OH)_2 \rightarrow CoO + H_2O \quad [6]$$

because no CoO peaks were observed in the XRD pattern (see Fig. 2). The theoretical weight loss to form CoO from $Co(OH)_2$ was about 19.4%, which was larger than the 14% obtained from the TGA results for the temperature change from 160 to 170°C (see Fig. 6). This difference was most likely caused by OH groups still remaining in the bulk within this temperature range, that could only be eliminated at higher temperatures. As the temperature was increased above 170°C, the oxidation of CoO to Co_3O_4 began to take place according to Eq. 7[29,30]

$$6CoO + O_2 \rightarrow 2Co_3O_4 \quad [7]$$

which was consistent with the XRD results, in that the intensity of the Co_3O_4 peaks increased with increasing temperature. According to the TGA results, this reaction was completed between 400 and 500°C.[29] The theoretical weight loss corresponding to the change from $Co(OH)_2$ to Co_3O_4 was about 13.6 %, but the weight loss obtained with the TGA during the temperature excursion from 150 to 450°C was about 17%. The difference was most likely associated with the removal of additional physisorbed/chemisorbed water at about 160°C.

In the temperature range from 170 to 400°C, primary amorphous CoO_x particles aggregated and formed larger secondary crystalline particles, thus eliminating some of the smallest intra- and interparticle voids and resulting in a sharp drop in the surface area and a gradual drop in the pore volume. These explanations are consistent with the XRD results shown in Fig. 2 and 3, which show that in the 200 to 400°C temperature range the average crystallite size more than doubled. In fact, the particle sizes of the xerogels obtained from the TEM images were larger than those estimated from the XRD results, which suggests that the particles seen in the TEM images consisted of an aggregate of crystallites, instead of single crystallites. This aggregation phenomenon occurred with minimal weight loss and an initial endothermic event that ceased at about 250°C (Fig. 6). This endothermic event was most likely caused by the decomposition of $Co(OH)_2$ to form CoO by elimination of chemisorbed water according to Eq. 6 and the subsequent oxidation of CoO to Co_3O_4 according to Eq. 7. Moreover, a significant structural change occurred in this temperature range, during which the xerogel converted from an essentially amorphous structure into an essentially crystalline structure. What was most interesting, however, is that in this temperature range, Fig. 5 shows that the skeletal density increased dramatically and attained nearly the theoretical density of Co_3O_4 at about 275°C, but the particle density was still increasing, thereby indicating the continued loss of surface area and pore volume.

In the final temperature range from 400 to 600°C, the secondary particles began to grow into even larger crystallites, which necessarily eliminated some of the large intra- and interparticle voids. As a result, the pore volume decreased continuously, but the surface area decreased more slowly. Again, the average crystallite size nearly doubled; and the results in Fig. 2 and 4 show that a highly crystalline Co_3O_4 structure was created at the final temperature of 600°C. The final weight loss and corresponding exothermic event that took place in this temperature range was assigned to structural relaxation,[31] a process whereby intra- and interparticle voids are eliminated but with little weight loss. During this structural relaxation, the surface area and pore volume of the CoO_x xerogel continuously decreased, but the crystallite size grew as shown in Fig. 1, 2, and 3.

It was also interesting to ascertain whether the Brunauer, Emmett, and Teller (BET) surface area corresponded to intra- or interparticle voids, depending on the calcination temperature. To illustrate, the CoO_x xerogels calcined at 250 and 600°C were selected with corresponding particle sizes of 15 and 35 nm (as determined from XRD) and skeletal densities of 4.10 and 5.74 g/cm^3, respectively. The external surface areas of these particles were calculated from the relationship

$$S = \frac{6}{D \cdot d_s} \quad [8]$$

where D is the particle diameter, d_s is the skeletal density, and S is the specific surface area; they were 98 and 30 m^2/g, respectively. For the xerogel calcined at 600°C, the calculated external surface area of 30 m^2/g was close to that obtained from the BET measurement of 20 m^2/g, indicating that the particles were nonporous and that both the BET surface area and pore volume were due to interparticle voids. In contrast, for the xerogel calcined at 250°C, the calculated external surface area of 98 m^2/g accounted for only half of the BET surface area of 180 m^2/g, indicating that significant intraparticle voids were present in the form of various sizes of pores. The highly porous structure of the CoO_x xerogels calcined below ca. 250°C was manifest through the sol-gel chemistry depicted in Eq. 1 and 2.

The sol-gel chemistry associated with transition metal alkoxides was also responsible for the unique electrochemical properties of the CoO_x xerogels, as shown in Fig. 7 to 10. For example, the very stable and reproducible peaks in the CVs shown in Fig. 7A and B between 0.3 and 0.5 V (vs. SCE) corresponded to the oxidation of CoOOH to CoO_2 according to Eq. 9[13]

$$CoOOH + OH^- \rightleftarrows CoO_2 + H_2O + e^- \quad [9]$$

where the CoOOH under open-circuit potential conditions was formed initially from[17]

$$Co(OH)_2 + OH^- \rightleftarrows CoOOH + H_2O + e^- \quad [10]$$

for the xerogels calcined at the lower temperatures, e.g., below 200°C; and from[17]

$$Co_3O_4 + H_2O + OH^- \rightleftarrows 3CoOOH + e^- \quad [11]$$

for the xerogels calcined at the higher temperatures, e.g., above 200°C.

To illustrate a charge-storage mechanism associated with the CoO_x xerogel electrodes, a theoretical capacitance, C_T, for the one-electron exchange redox reaction (Eq. 9) that is assumed to take place only on the surface of each particle was estimated from

$$C_T = \frac{sF}{h^2 L_A \Delta V} \quad [12]$$

where s is the specific surface area, F is Faraday's constant, h is the length of a crystal lattice and taken as 4.26 Å

for crystalline CoO,[28] L_A is Avogadro's number, and ΔV is the potential range from 0 to 0.5 V for the current measured. Equation 12 implies that there is only one Co atom in the square area of h on the surface; thus, at 150 and 300°C, corresponding surface areas of 199 and 99 m^2/g give rise to C_T of 351 and 175 F/g, respectively. These values are very close to the measured capacitances of 291 and 163 F/g at these two temperatures, respectively. This result suggested that the CoO_x redox reaction was taking place only on the surface of each particle that was in direct contact with the electrolyte, and that the charge-storage mechanism was based solely on the surface redox reaction and thus pseudocapacitance. Moreover, if the reaction involved all of the bulk material, a specific capacitance of 2100 F/g would have been observed, which is about six to seven times the theoretical capacitance. This result implies that 14 to 17% of the material was utilized for energy storage, a fairly large percentage for a surface redox reaction. This unique feature of the CoO_x xerogels was attributed to the high surface area of this sol-gel-derived cobalt oxide.

According to the literature,[13,17] the anodic shoulder in the CVs shown in Fig. 7A and B for the xerogel calcined at 150°C was associated with the oxidation process given in Eq. 10, whereas the cathodic shoulder corresponded to the reverse of Eq. 10. This very stable redox reaction (Fig. 7B), which disappeared at higher temperatures, most likely gave rise to the very high capacitance observed with this material (291 F/g). The appearances of these CV curves were also very similar to those reported by Boggio et al.[13] for a Co_3O_4 thin film deposited by thermal decomposition of $Co(NO_3)_2$ on a titanium support, which further substantiates that the origin of the capacitance in these bulk cobalt oxide materials is due solely to surface redox reactions depicted by Eq. 9 to 11, as explained in more detail elsewhere.[13] Figure 7A also shows that with an increase in temperature, both of the anodic and cathodic shoulders disappeared; and the peak currents of both the cathodic peak at 0.3 V and the corresponding anodic peak decreased with increasing calcination temperature, indicating that crystalline, nonelectrochemically active species with a smaller active surface area had been formed. At the highest calcination temperature, the anodic potential limit extended fully into the oxygen evolution region, indicating that the only process occurring on the surface was the formation of oxygen.

The discharge curves shown in Fig. 9 are also explained by taking into account the structure and electrochemically active surface area of the CoO_x xerogels. According to Fig. 2, the electrodes prepared with the CoO_x xerogels calcined at the lower temperatures had an amorphous structure of $Co(OH)_2$. Thus, the high intraparticle surface area of this amorphous material contributed to the large charging and discharging currents observed in the potential range from 0 to 0.3 V. However, at temperatures above 200°C, the xerogel was converted into a crystalline structure of Co_3O_4 that resulted in a decrease of the electrochemically active surface area. Consequently, a loss in capacity was observed for all materials prepared at temperatures above 200°C (see Fig. 9). These results suggested that the surface area played a major role in controlling the electrochemical properties of the CoO_x xerogel electrodes. The highest surface area electrode (calcined at 150°C) had the highest redox current, because of its unique amorphous structure. These trends were also apparent in Fig. 10, where the amorphous structure of the CoO_x xerogel electrode calcined at 150°C resulted in the highest specific capacitance of all of the CoO_x xerogels studied.

Conclusions

The calcination temperature had a significant impact on the structure of the sol-gel derived CoO_x xerogel powders and their corresponding electrochemical properties. The xerogels essentially exhibited both high surface area and pore volume at relatively low calcination temperatures; but after some characteristic calcination temperature was exceeded, both the surface area and pore volume decreased with an increase in temperature. The maximum surface area and pore volume were observed for the xerogel calcined at 150°C, which yielded a unique amorphous structure of $Co(OH)_2$. At calcination temperatures above 160°C, however, the amorphous $Co(OH)_2$ began to decompose to form CoO that was subsequently oxidized to form crystalline Co_3O_4 with an increase in temperature, thereby resulting in lower surface areas and pore volumes. The electrochemical study showed that the xerogel electrode calcined at 150°C was very stable over several thousand charging/dischaging (CV) cycles, and it exhibited the highest surface redox currents, which were clearly associated with the high surface area and pore volume of the amorphous $Co(OH)_2$ structure. However, the redox currents began disappearing at temperatures above 200°C, as a result of structural changes that took place during formation of the crystalline Co_3O_4 and the corresponding decreases in the surface area and pore volume. The highest average specific capacitance obtained was 291 F/g for a single electrode, and it corresponded to the CoO_x xerogel electrode calcined at 150°C. This result was very close to the theoretical capacitance of 351 F/g that was obtained based on a surface redox mechanism; thus, the charge-storage mechanism was due solely to a surface redox reaction. The unique physical and electrochemical properties of these CoO_x xerogels were attributed to the sol-gel chemistry of transition metal alkoxides.

Acknowledgments

This material is based upon work supported in part by the U.S. Army Research Office under grant no. DAAH04-96-1-0421 and in part by the U.S. Department of Energy under cooperative agreement no. DE-FC02-91ER75666.

Manuscript submitted January 20, 1998; revised manuscript received July 17, 1998.

The University of South Carolina assisted in meeting the publication costs of this article.

REFERENCES

1. B. E. Conway, *J. Electrochem. Soc.*, **138**, 1539 (1991).
2. B. E.Conway, in *Third International Seminar on Double Layer Capacitors and Similar Energy Storage Devices*, Vol. 3, Florida Educational Seminar, Inc., Boca Raton, FL (1993).
3. S. Trasatti and P. Kurzweil, *Plat. Met. Rev.*, **38**, 46 (1994).
4. S. Sarangapani, B. V. Tilak, and C. P. Chen, *J. Electrochem. Soc.*, **143**, 3791 (1994).
5. I. D. Raistrick, in *Electrochemistry of Semiconductors and Electrodes*, J. McHardy and F. Ludwig, Editors, p. 297-355, Noyes Publications, Park Ridge, NJ (1992).
6. A. Rudge, I. Raistrick, S. Gottesfeld, and J. Ferraris, *Electochim. Acta*, **39**, 279 (1994).
7. J. P. Zhang, P. J. Cygan, and T. R. Jow, *J. Electrochem. Soc.*, **142**, 2699 (1995).
8. K. C. Liu and M. A. Anderson, *J. Electrochem. Soc.*, **143**, 124 (1996).
9. V. Srinivasan and J. W. Weidner, *J. Electrochem. Soc.*, **144**, L210 (1997).
10. V. S. Bagotsky, N. A. Shumilova, and E. I. Khrushcheva, *Electochim. Acta*, **21**, 916 (1976).
11. C. Iwakura, A. Honji, and H. Tamura, *Electochim. Acta*, **26**, 1319 (1981).
12. S. Trasatti, *Electochim. Acta*, **29**, 1503 (1984).
13. R. Boggio, A. Carugati, and S. Trasatti, *J. Appl. Electrochem.*, **17**, 828 (1987).
14. E. Zhecheva, R. Stoyanova, M. Gorova, R. Alcantara, J. Morales, and J. L. Tirado, *Chem. Mater.*, **8**, 1429 (1996).
15. R. N. Singh, J. F. Koenig, G. Poillerat, and P. Chartier, *J. Electrochem. Soc.*, **137**, 1408 (1990).
16. T. Maruyama and S. Arai, *J. Electrochem. Soc.*, **143**, 1383 (1996).
17. F. Svegl, B. Orel, M. G. Hutchins, and K. Kalcher, *J. Electrochem. Soc.*, **143**, 1532 (1996).
18. I. Serebrennikova and V. I. Birss, *J. Electrochem. Soc.*, **144**, 566 (1997).
19. C. J. Brinker and G. W. Scherer, *Sol-Gel Science*, Academic Press, San Diego, CA (1990).
20. P. J. Davis, C. J. Brinker, D. M. Smith, and R. A. Assink, *J. Non-Cryst. Solids*, **142**, 197 (1992).
21. C. Lin and J. A. Ritter, in *Fundamentals of Adsorption*, M. D. LeVan, Editor, Kluwer Academic Publishers, Boston, MA (1996).

22. C. Lin, J. A. Ritter, and M. D. Amiridis, *J. Non-Cryst. Solids*, **215**, 146 (1997).
23. E. M. Rabinovich, in *Sol-Gel Technology for Thin Films, Fibers, Preforms, Electrons and Specialty Shapes*, L. C. Klien, Editor, Noyes Publications, Park Ridge, NJ (1988).
24. W. F. Maier, I. C. Tilgner, W. Wiedron, and H. C. Ko, *Adv. Mater.*, **5**, 726 (1993).
25. F. Svegl and B. Orel, J. *Sol-Gel Sci. Technol.*, **8**, 765 (1997).
26. Y. Takasu, S. Onoue, K. Kameyama, Y. Murakami, and K. Yahikozawa, *Electrochim. Acta*, **39**, 1993 (1994).
27. H. P. Klug and L. E. Alexander, *X-Ray Differaction Procedures*, John Wiley & Sons, New York (1962).
28. *CRC Handbook of Chemistry and Physics*, 62nd ed., R. C. Weast and M. J. Astle, Editors, CRC Press, Inc., Boca Raton, FL (1981-1982).
29. F. A. Cotton and C. Wilkinson, *Advanced Inorganic Chemistry-A Comprehensive Test*, 4th ed., John Wiley & Sons, Inc., New York (1980).
30. M. Pourbaix, *Atlas of Electrochemical Equilibria in Aqueous Solutions*, p. 325, NACE, Houston, TX (1974).
31. G. W. Scherer, *Relaxation in Glasses and Composites*, John Wiley & Sons, Inc., New York (1986).

Characterization of Electropolymerized Polyindole

Application in the Construction of a Solid-State, Ion-Selective Electrode

P. C. Pandey and R. Prakash[a]

Department of Chemistry, Banaras Hindu University, Varanasi-221 005, India

ABSTRACT

The characterization of polyindole made by anodic electropolymerization of indole monomer in dichloromethane is reported based on scanning electron microscopy (SEM) and differential scanning calorimetry (DSC). The results on SEM show that the granules in the polymer film are arranged in an ordered manner. The domain of the nuclei in the film made under potentiostatic condition is much smaller as compared to the domain of the nucleation in the polymer film made under potentiodynamic condition. The DSC data shows that the polymer is stable at higher temperature. A solid-state potassium ion-selective electrode (ISE) using polyvinyl chloride (PVC) matrix membrane impregnated with valinomycin at the surface of the polyindole-modified electrode is reported. Neutral-carrier impregnated PVC membrane is formed by casting over the surface of the polyindole-modified electrode. The resulting ISE without the incorporation of polyanions in the polyindole film shows high selectivity to K^+ with negligible drift of the baseline potential with a slope of 59 mV/dec within Nernstian behavior. The detection limit of the potassium ion sensor is 6×10^{-6} M with a wide linearity over almost 5 dec. Typical responses of the neutral-carrier impregnated PVC membrane over the polyindole-modified electrode to potassium ion is reported.

Introduction

The electrochemical synthesis of polyindole has received a significant share of attention during recent years.[1-9] Recently we have reported the electrochemical synthesis of polyindole by anodic oxidation of indole monomers in dichloromethane[9] containing tetrabutylammonium perchlorate. The resulting polymer shows better stability and improved conductivity as compared to the polymer synthesized earlier.[1,2] The application of the polymer in the construction of rechargeable batteries has been reported.[9] However, the results of the surface structure and stability of the film at higher temperature were not reported. The results based on scanning electron microscopy (SEM) and differential scanning calorimetry (DSC) of the polymer film, made by electropolymerization of polyindole in dichloromethane, are reported in this present communication.

Over the last 35 years development of ion-selective electrodes (ISEs) has grown at an ever-increasing rate due to their need in various spheres of life, particularly in the analytical, biological, and clinical areas. Accordingly, extensive studies have been made on the development of ISEs based on unblocked (with conventional single/double-barrel configuration) and blocked (coated wire electrode, CWE) interfaces. Extensive investigations on ISEs based on unblocked interfaces have been made, several of them on a commercial scale. However, the problems with such a configuration exist in the applications, mainly due to (*i*) use in upright position and (*ii*) use of internal filling solution and internal reference element. The coated wire electrodes have gained attention due to the simplicity involved in the construction of the ISEs, avoiding the problems associated with single/double-barrel configuration. However, there still exists a need for further research to overcome the problems associated with the drift and overshoot of the potential leading to the variable baseline (stead-state potential) recovery during the potentiometric operation. A significant share of attention on these problems has been paid during last few years.[10-15] The application of conducting polymers[10-15] has been demonstrated along these lines. Quite recently[10] all-solid-state potassium-ion-selective electrodes have been reported on a Pt disk using a bilayer film of polypyrrole/poly(4-styrenesulfonate) (PPy/PSS) composite covered with a plasticized polyvinyl chloride (PVC) matrix membrane impregnated with valinomycin. The problem associated with the overshoot of the baseline potential was reduced due to the electroactivity and cation-exchange behavior of the PPy/PSS film, resulting in the formation of the concentration cells also referred to as symmetric cells (ions-in, ions-out) at the test solution/PVC and PVC/(PPy/PSS) interfaces. Because of the high thermal stability and good electroactivity of the polyindole, it is of great interest to study the potentiometric behavior of polyindole-modified electrode in the construction of ISEs. This is attempted in the present communication. An ISE for potassium ion using valinomycin-impregnated, plasticized PVC over the surface of polyindole-modified electrode is reported.

Experimental

Indole (analytical reagent grade), PVC powder, dibutyl phthalate, and valinomycin were obtained from Aldrich Chemical Co. Tetraphenyl borate was obtained from E-Merck, India, Ltd; tetrabutylammonium perchlorate (TBAP) was obtained from Sigma Chemical Co. TBAP was dried in a drying piston below 100°C for a period of 24 h under vacuum. The aqueous solutions were prepared in double-distilled deionized water.

The electrochemical synthesis of polyindole was performed with a Solartron electrochemical interface (model

[a] Present address: ITRC, M.G. Marg., Lucknow, India.